# Seismic velocity changes, strain rate and non-volcanic tremors during the 2009-2010 slow slip event in Guerrero, Mexico

Diane Rivet[1*], Michel Campillo[1], Mathilde Radiguet[1], Dimitri Zigone[1], Victor Cruz-Atienza[2], Nikolai M. Shapiro[3], Vladimir Kostoglodov[2], Nathalie Cotte[1], Glenn Cougoulat[1], Andrea Walpersdorf[l], Eric Daub[1]

[1] ISTerre, Université Joseph Fourier, Maison des Géosciences, BP 53, 38041 Grenoble, France

[2] Instituto de Geofísica, Universidad Nacional Autónoma de México, CU, Coyoacan, 04510 México, D.F., México.

[3] Institut de Physique du Globe de Paris, Sorbonne Paris Cité, CNRS (UMR7154), 1 rue Jussieu, 75238 Paris, cedex 5, France.

* now at Institut de Physique du Globe de Paris, Sorbonne Paris Cité, CNRS (UMR7154), 1 rue Jussieu, 75238 Paris, cedex 5, France.

Abbreviated title:

**Seismic velocity changes and NVTs during a slow slip event**

Corresponding author is Diane Rivet :

Tel: +33 (0)1 83 95 75 71

Fax :+33 (0)1 83 95 77 17

Email address : diane.rivet@ujf-grenoble.fr

## Summary

We use ambient noise cross-correlations to monitor small but reliable changes in seismic velocities and to analyze non-volcanic tremor (NVT) intensities during the slow slip event (SSE) that occurred in 2009 and 2010 in Guerrero. We test the sensitivity of the seismic velocity to strain variations in absence of strong motions. The 2009-2010 SSE presents a complex slip sequence with two sub-events occurring in two different portions of the fault. From a seismic array of 59 seismometers, installed in small antennas, we detect a velocity drop with maximum amplitude at the time of the first sub-event. We analyze the velocity change at different period bands and observe that the velocity perturbation associated with the SSE maximizes for periods longer than 12 s. Then a linearized inversion of the velocity change measured at different period bands is applied in order to determine the depth of the portion of the crust affected by this perturbation. No velocity change in the first 10 km is detected. Below, the velocity perturbation increases with depth, affecting the middle and lower crust. Finally we compute the transient deformation produced by the SSE in an elastic model using the slip evolution recovered from the inversion of continuous GPS. The comparison between the velocity changes and the deformation suggests that the velocity change is correlated with the strain rate rather than with the strain. This result is similar to what was observed during the 2006 SSE in the same region and suggests a non-linear behavior of the crust.

The velocity changes can be interpreted together with other observables such as non-volcanic tremors. During the 2009-2010 SSE we measure non-volcanic tremor activity using continuous seismic records filtered between 2 and 8 Hz. We observe a correlation between velocity changes (for period band greater than 14 s) and tremor activity whereas no correlation exists between velocity changes and seismic noise energy measured at long

periods. These observations suggest that both seismic velocity change and non-volcanic tremor can be used as indication of transient deformation at depth.

**Keywords:** Coda waves, Wave scattering and diffraction, Rheology and friction of fault zones, Subduction zone processes

# 1 Introduction

Non-volcanic Tremor (NVT) and Slow Slip Events (SSE) are observed in many active plate boundaries around the world (e.g. review of Schwartz & Rokosky 2007). SSEs are transient aseismic slips that contribute to release the accumulated elastic strain at the plate interfaces. SSEs are usually accompanied by NVT episodes, which are weak seismic signals of long duration, persistent in time and coherent over many stations (Obara 2002; Rogers & Dragert 2003; Obara *et al.* 2004). The data acquired on these two geophysical processes reveal a wide diversity of behaviors that vary from one region to another. For instance, in Cascadia and Southwest Japan subduction zones a clear temporal and spatial correlation between NVT and SSE has been observed and called Episodic Tremors and Slip (ETS) (Rogers & Dragert 2003; Obara *et al.* 2004). In other subduction zones like Costa Rica (Brown *et al.* 2005), Alaska (Ohta *et al.* 2006; Peterson & Christensen 2009) and Mexico (Payero *et al.* 2008; Kostoglodov *et al.* 2010) the association of SSE and NVT does not seem systematic. Moreover, in areas like the Hikurangi subduction margin, New Zealand (Delahaye *et al.* 2009; McCaffrey *et al.* 2008), and the Boso Peninsula of Japan (Ozawa *et al.* 2007), even no NVT was observed during slow slip. However, the recent detection of NVT at the northern Hikurangi margin associated with the 2010 Gisborne SSE suggests that the thick accumulation of highly attenuating sediment in the accretionary wedge inhibits the NVT detection in some cases (Kim *et al.* 2011). According to the classification proposed by Obara

72 (2011), SSEs in Mexico belong to long-term SSE considering their duration and their updip
73 position in the trench as shown by Vergnolle *et al.* (2010) and Radiguet *et al.* (2011). Long-
74 term SSEs are also observed in the Bungo Chanel in Southwest Japan and trigger neighboring
75 downdip NVT activity (Hirose *et al.* 2010). The authors suggest that long-term SSE could
76 activate downdip short-term SSEs, which could remain undetected by GPS, and synchronized
77 with NVT. Besides, some studies locate tremors at the plate interface as suggested in Japan
78 (e.g. Shelly *et al.* 2006; Ohta *and Ide* 2008), while in other studies it was proposed that they
79 are located within the over-riding plate like in Cascadia (Kao *et al.* 2005), Japan (Nugraha &
80 Mori 2006) and Mexico (Payero *et al.* 2008). However this discrepancy in the depth of NVTs
81 in those subduction zones may arise from the locating methods. Different mechanical
82 processes are invoked to explain tremor's generation, but an accurate NVT depth estimate is
83 required to discriminate their possible physical models. The two predominant models of
84 NVT, as described by Rubinstein *et al.* (2010) are: (1) frictional processes with shear rupture
85 of some portion of a fault undergoing slow slip; and (2) fluid processes, with fluid flow at the
86 plate interface and within the overlying plate. For the later model deshydratation from basalt
87 to eclogite of the subducting slab would increase the fluid pressure causing sequence of
88 hydraulic fracturing recorded at the surface as long and emissive seismic signals (Obara *et al.*
89 2002). Rogers & Dragerts (2003) argue that the resonating walls of fluid conduits near the
90 plate interface could also produce tremor like signals recorded at the surface.
91 In the Guerrero region, Mexico, several observations suggested a complex behavior of NVT
92 activity in relation with SSEs. The 2006 SSE that occurred in the region had a significant
93 seismic moment magnitude ($M$w=7.4 for the 2006 event according to Radiguet *et al.* (2011)
94 and Larson *et al.* (2007)). During this SSE, the activity of the NVT increased but the NVT
95 area was separated spatially from the slipping portion of the interface (Kostoglodov *et al.*
96 2010). Besides, significant NVT episodes occurred during the inter-SSE period (Kostoglodov

97 *et al.* 2010). Finally, Rivet *et al.* (2011) observed a transient velocity change during this SSE
98 that was strongly correlated with the maximum of the dilation rate induced by the SSE, and
99 that they interpreted as a nonlinear elastic response of the crust.

100 In this present work we investigate the relation between seismic velocity changes, and the
101 NVT activity during the 2009-2010 SSE. We will focus particularly on the relation between
102 changes of velocity, the deformation produced by the SSE, and the NVT activity. For this
103 purpose, we propose to use seismic velocity changes as a proxy of the strain rate.

104 The 2009-2010 SSE started in July 2009 (Walpersdorf *et al.* 2011). The surface
105 displacements observed from the GPS time series are lower than those observed during the
106 2006 SSE (Walpersdorf *et al.* 2011). However the slip duration for this SSE is longer, about
107 14 months against 6 months for the previous event. It also presents a more complex slip
108 sequence. From GPS observations, Walpersdorf *et al.* (2011) and Radiguet (2011) showed
109 that the SSE broke in two steps, with two separate portions of faults that have dislocated
110 successively. The first event broke a patch of the subduction interface located in the
111 southwest part of the Guerrero state and the second one started at the end of February 2010
112 and took place in the southeast part of Guerrero (Figure 1). Zigone *et al.* (2012) proposed that
113 this second subevent was actually triggered by teleseismic surface waves generated by the
114 giant M8.8 Maule (Chile) earthquake of 2010. The 2009-2010 SSE is thus interesting in the
115 sense that it allows to assess the sensitivity of the detection of small crustal velocity
116 perturbation during this complex SSE, which has a smaller slip rate than the 2006 SSE
117 (40cm/yr versus ~70cm/yr).

118 These observations of velocity change during the SSE are important for two reasons: first,
119 velocity changes are clearly related to the strain rate perturbation produced at depth by the
120 SSE. Second, using velocity changes as a proxy of the strain rate, we can investigate the
121 relation between NVT and the state of deformation of the overriding plate.

# 2 Data and method

## 2.1 Seismological data

We use seismic records from a temporary network of nine seismic mini-arrays deployed since 2009 in the framework of the French – Mexican G-GAP project (Table 1) complemented with four broadband stations of the Mexican National Seismological Service (SSN) network (Table 2). Four mini-arrays consist of a broadband sensor (CMG40 of Guralp) in the center, surrounded by 6 or 3 short period sensors with an aperture of approximately 150 m, e.g. XALI mini-array (Figure S1). The other five mini-arrays consist of groups of 3 to 6 short period sensors. Overall, we have 59 sensors (8 broadband) located nearby the city of Iguala in the northern part of the Guerrero state (Figure 1). Although we have a rather dense array, recording periods vary from one station to another and not always cover the entire duration of the SSE. We measure velocity changes for the period band between 4 and 27 s, however, most of the sensors we use in this study are short period sensors. At long period, the instrument responses of those sensors show an important bias in the phase and error in the amplitude of the signal. However, because these errors are constant over time, they do not affect the relative inter-station phase shift we measure on the noise cross-correlations. Brenguier *et al.* (2008a,b) demonstrated the feasibility of using exclusively short period sensors to measure velocity changes on the San Andrea fault in the Parkfield area and on the Piton de la Fournaise volcano at La Reunion island. In this present analysis we make reliable measure down to 27 s using mainly short period sensors.

The procedure for data processing and computing seismic noise correlations in different period bands is described thereafter. After high-pass filtering, we eliminate portion of signals with amplitude greater than 10 times the standard deviation calculated for the day. We then

146 apply spectral whitening between 1 and 30 s on all daily noise records. We bandpass filter
147 continuous signals in 2 period ranges: 4-16 s and 8-30 s. To remove small earthquakes,
148 signals with amplitude greater than 3 times the standard deviation are then discarded. Finally,
149 we apply 1-bit temporal normalization on the two sets of noise signals filtered in the period
150 band 4-16 s and 8-30 s. By doing so we prevent bias due to the 1-bit normalization that can
151 occur if applied on broadband signals. Records are then correlated for all pairs of stations and
152 for everyday. We obtain two sets of correlations in the two period bands 4-16 s and 8-30 s. To
153 measure seismic velocity variations, we bandpass filter the correlations in different period
154 bands (Table 3). For all period bands lower than the 13-17.9 s period band, we used
155 correlations measured from the noise filtered in the 8-30s period band. We often refer to the
156 central period, which is the center of the period band of the cross-correlations.
157

158 ## 2.2 Measurements of velocity change

159 Seismic velocity changes in the Earth's crust indicate changes in the elastic properties
160 related to the stress field variations in time. A continuous monitoring of the seismic velocity
161 within the crust thus provides a measure of the mechanical state of the crust. This continuous
162 monitoring is achieved through the use of seismic noise, which illuminates continually the
163 crust. The possibility to recover Green's functions from the cross-correlations of random
164 seismic wavefields such as seismic coda (Campillo and Paul, 2003) and seismic noise
165 (Shapiro & Campillo 2004) has been recently demonstrated. From the monitoring of the
166 reconstructed seismic waves travel times it is possible to recover the relative seismic velocity
167 change in the area of interest. A robust feature of this seismic noise based technique is that
168 reliable measures of velocity changes can be achieved even when the full reconstruction of

169 the Green's function from the cross-correlation has not been reached yet (Hadziioannou *et al.*
170 2009; Weaver *et al.* 2009).

171 From continuous seismic noise records we compute correlations between all pairs of
172 stations in the Guerrero region for consecutive periods of time. These correlations are
173 calculated between vertical components over a 40-day window that is shifted every 10 days,
174 from May 2009 to May 2011. From the correlations computed from the vertical components
175 of noise records, we retrieve mainly Rayleigh waves. Figures S2 presents the 40-day cross-
176 correlation functions computed between two broadband stations and two short period sensors.
177 The stability of the cross-correlations for the long period 8-30 s between short period sensors
178 is compared to the one obtained from broadband sensors. It can be observed that the bias in
179 the phase introduced by the short sensors is constant and that later arrivals in the coda of the
180 cross-correlations are stable over time.

181 The reference cross-correlation, for a given pair of stations is defined as the average of all
182 correlations during the entire recording period. This reference can be interpreted as the
183 average background state of the surrounding medium. Using the same approach as for
184 repeating earthquakes (e.g. Poupinet *et al.* 1984), seismic velocity change is obtained from the
185 comparison of the current cross-correlation function, computed for a given time, with the
186 reference cross-correlation. Under the first-order assumption of a homogeneous perturbation
187 in the crust, the relative difference in travel time gives the relative change in the seismic
188 velocity: $dv/v = -dt/t$.

189 For any couple of reference cross-correlation and current cross-correlation functions, the
190 time delay between the two signals is measured on the coda waveforms from multiply
191 scattered waves. It exists two different approaches to measure these delays. First, the
192 Stretching method proposed by Lobkis & Weaver (2003) in laboratory ultrasonics, consists in
193 stretching the whole coda of the current signal by a factor $\varepsilon$until the correlation coefficient

194 between this signal and the coda of the reference reaches a maximum. For this particular
195 value of the ε we retrieve the temporal dilation $\varepsilon = dv/v$. The distortion between two waves
196 form is given by the maxima of the correlation coefficient if less than 1.
197 Second, the Multiple window Spectral Analysis method originally proposed by Poupinet *et al.*
198 1984, also called Doublets method (*e.g.* Brenguier *el al.* 2008a,b) measures apparent delays
199 $dt(t)$ within a series of short time overlapping windows at several distinct time $t$. These
200 $dt(t)$ are determined from the phase shift measurements and a cross spectrum analysis in the
201 frequency domain. The slope $dt(t)$ of the distribution of $dt(t)$ measures reveals a change in
202 the medium $dv/v = -dt/t$. A measure of a coherency between two windowed signals on the
203 coda allows to eliminate signals with insufficient signal to noise ratio. In addition, a least-
204 squares error is estimated for each distribution of $dt(t)$ for every cross-correlations. In this
205 approach, the delay is independent of the fluctuations of the energy spectrum of the
206 correlation. Finally, we average the relative velocity changes for all pairs of stations and
207 repeat this computation for different period bands. In the doublet method, the reliability of the
208 velocity change measurements is estimated from both the coherency measured between the
209 reference and the 40-day stacked cross-correlation functions and the statistical error of the
210 linear regressions $dt(t)$ averaged for all the correlations (Clarke *et al.* 2011).
211 A major limitation of the seismic noise correlation method to monitor geological
212 structures comes from the irregular distribution of noise sources and their variations over
213 time. Noise sources in the microseismic period ranges are mainly concentrated in oceanic
214 regions (Stehly *et al.* 2006; Tanimoto *et al.* 2006; Koper *et al.* 2009; Stutzmann *et al.* 2009;
215 Landes *et al.* 2010; Schimmel *et al.* 2011; Hillers *et al.* 2012) and depend on seasons and
216 climatic events such as storms. In Supplementary Materials (see Figure S3), we propose a
217 study of the normalized background seismic energy flow and its variations over time in the
218 period band we use in the velocity changes analysis.

Weaver *et al.* (2009) and Froment *et al.* (2010) showed that the anisotropic distribution of noise could produce an error of 1% in the measurement of travel times for the ballistic waves reconstructed from the noise cross-correlations. On the other hand, the change in travel time induced by a change in velocity of the medium is less than 1% (e.g. Wegler & Sens-Schonfelder, 2007; Brenguier *et al.* 2008a, b; Chen *et al.* 2010; Rivet *et al.* 2011). It is therefore essential to overcome the bias introduced by seasonal variations of noise sources.

To reduce the errors caused by possible variations of the noise source positions, we measure the travel time delays on coda waves of the correlations. The coda window is defined between 5 s after the arrival of the direct wave and 90 s. The coda is made up of diffuse waves scattered on the heterogeneities of the crust and thus tend to lose the source signature. Travel time delay measured within the coda is less sensitive to source variations.

### 2.3 Selection of correlations based on their signal to noise ratio

We use the signal to noise ratio estimations to make an automatic selection of daily correlations. From the reference correlation computed between two stations, we measure the time of the maximum of the envelope signal. This gives us a good approximation of the position of the Rayleigh wave reconstructed for each daily correlation. We then calculate the average amplitude of the Rayleigh wave for each daily correlation on a 20s window centered on the maximum amplitude with respect to the average amplitude of the incoherent signal (noise) measured for long time lapse on a window of 50 s between 190 and 240 s of the correlation signal. Daily correlations with a signal to noise ratio greater than 1.5 are then averaged over periods of 40-day with an overlap of 10 days to obtain stable traces with higher signal to noise ratio. Figure S4 presents daily cross-correlations for the AMAC3-APAX4 pair of stations before and after the selection based on the signal to noise ratio. By averaging the

243 daily correlations over 40 days, the signal to noise ratio increases by a factor $\sqrt{40} \approx 6$. We
244 thus expect the stacked signals to reach a signal to noise ratio greater than 10.
245

246 ### 2.4 Reliability of the velocity change measurements

247 The seismic network used in this study consists of broadband and short period stations
248 belonging to two separate networks with important variations over time of the number of
249 stations available. We use both the Multiple Window Spectral Analyze method and the
250 Stretching method described above to check the reliability of our velocity change
251 measurements. Changes over time are estimated from all 40-days stacks of cross-correlations
252 in the 8-20 s period band. The results obtained with both methods are in good agreement
253 (Figure S5). This confirms the robustness of the measured travel time changes despite the
254 large variations over time of the number of pairs of stations (Figure 2c).
255 Weaver *et al.* (2011) established a theoretical expression to estimate the error of velocity
256 change computed on noisy measurements. This expression is a function of the central
257 frequency, the bandwidth, the length of the windowed coda and the coherency between the
258 stretched correlation at a given time and the reference one. For correlations computed from
259 consecutive period of 40 days of noise at 8-20 s period band, using the theoretical expression
260 of Weaver *et al.* (2011) we find that the velocity change fluctuation due to the noisy
261 component of the signals we use is $1.8\times10^{-3}$ while the largest variation observed during SSE
262 reaches $8\times10^{-3}$.
263
264

265 ## 3 Results

266 A long-term variation of seismic velocity is observed during the SSE (Figure 2). This SSE

267 does not emit any seismic waves susceptible to affect the surface layers of the crust and cause
268 superficial velocity change. Similarly to the 2006 SSE (Rivet *et al.* 2011), the 2009-2010 SSE
269 affects the medium at depth only through the slow deformation it produces. However the GPS
270 time series during this SSE show that the SSE had a complex slip sequence with two portions
271 of the fault that slipped successively (Walpersdorf *et al.* 2011; Radiguet 2011). Figure 2a
272 presents the surface displacements during the SSE at the GPS stations CPDP and CAYA
273 (GPS locations are shown in Figure 1). The first sub-event that occurred on the western part
274 of the Guerrero subduction interface produced a slip that started in mid-2009 and was
275 detected on CAYA station, whereas the second sub-event, that happened on the eastern part
276 produced a slip that started in early March 2010 and was detected on stations located to the
277 east, e.g. CPDP. Figure 2b shows the seismic velocity evolution estimated in the 15-20 s
278 period band during the SSE. We observe a decrease of about 0.8% of the seismic velocity
279 between September and November 2009 during the first sub-event. The seismic velocity
280 changes observed here do not correlate with the number of available station pairs (Figure 2c).
281 Besides, to verify that the velocity change at long period is reliably measured using mainly
282 short period sensors, we compare the velocity change from 7 broadband stations with the
283 velocity change measured from 51 short period sensors (Figure S6). Despite higher
284 fluctuation of the velocity change measurements due to a limited number of correlations, the
285 main perturbation between September and November 2009 is detected for each subset of
286 stations.

287 Radiguet (2011) was able to model the evolution of the slip on the subduction interface
288 during the SSE (Figure S7) from the GPS time series inversion using the Principal
289 Component Analysis Inversion Method (PCAIM) developed by Kositsky & Avouac (2010).
290 Through a comparison between the variations of seismic velocity (Figure 2b) and the slip
291 velocity of the SSE (Figure S7), we observe that the major reduction in wave speed

292 corresponds to the period of highest slip rate between September and November 2009.

293 ### 3.1 Seismic velocity changes at different frequency bands

294 To constrain the extension of the velocity perturbation at depth, we measure the seismic
295 velocity changes using the records filtered in different period bands listed in table 3, from 4-
296 5.6 s to 20-27 s (Figure 3). It has been shown both theoretically and observationally that the
297 seismic coda has average properties described by the equipartition of the propagation modes
298 (Hennino *et al.* 2001; Margerin *et al.* 2009). As a result, the coda recorded at the surface is
299 dominantly composed of surface waves. In the case of noise cross-correlations computed
300 from the vertical component records, we recover mainly Rayleigh waves. The global
301 sensitivity of coda wave to velocity changes at depth in a given time window depends on the
302 proportion of the travel time spent as each type of waves for all contributing paths. At the first
303 order, we consider only the dominant surface waves and we expect that the travel time delays
304 measured on the coda of the cross-correlation functions depend on periods similarly to the
305 surface waves: shorter periods are sensitive to shallower structures while longer periods
306 sample deeper in the crust. This hypothesis is supported by numerical tests on the sensitivity
307 of coda waves delayed by a velocity change at depth (Obermann *et al.* 2013). The authors
308 investigated the sensitivity at depth of the coda waves to local velocity perturbation in a 2D
309 numerical wave-field simulation. They showed that the depth sensitivity of the coda waves is
310 a combination of bulk-wave sensitivity and surface-wave sensitivity. The partitioning ratio of
311 bulk and surface-wave sensitivities depends on the lapse time in the coda among other factors.
312 Surface waves dominate the coda sensitivity for about six mean free times, while body waves
313 dominate the later coda. The Earth's crust is a weakly scattering medium with long mean free
314 times for long period seismic waves (e.g. >5s) – in fact teleseismic records indicate that the
315 long-period waves remain coherent for long travel times. Working at low frequency and at

316 early times in the coda as it is done here implies that our observations of velocity changes can
317 be interpreted using the sensitivity of surface-wave. Therefore, the depth sensitivity of the
318 velocity change measurements during the SSE can be approximated by surface-waves
319 sensitivity. Velocity variations obtained for periods around 14 s have a high sensitivity within
320 the middle crust but this sensitivity decreases toward the subduction interface (~40 km in
321 Guerrero), (Figure S8). Therefore, variation in speed measured at around 14 s period indicates
322 a significant change of the medium induced by deformation at mid-crustal depth.
323 During the 2009-2010 SSE for central periods smaller than 8 s, velocity fluctuations are
324 smaller than the noise level (-0.1%) implying that we detect no measurable seismic velocity
325 variations (Figure 3a). On the other hand, for wave speed variations calculated at periods
326 between 8 and 18 s of central period, there was a rapid decrease of the seismic velocity in July
327 2009. Although this variation has large amplitudes (-0.8%), the perturbation disappeared after
328 about 3 months. It is impossible to detect precisely the onset of this perturbation because no
329 sufficient data were acquired before July 2009. After the velocity rises close to its average
330 value in August, a long and major seismic velocity decrease affects the medium between
331 September and November 2009. This perturbation that reaches -0.8% is particularly visible
332 between for all period bands between 12 and 24 s of central period. At longer period, beyond
333 24 s, it is possible that this decrease of velocity still exists. However, with our dataset
334 dominated by short period sensors, the measurement of the velocity perturbation becomes
335 unstable at long periods. Besides, weak scattering at long period limits the signal to noise
336 ratio in the coda because of the lack of late energetic arrivals which would accumulate delays
337 large enough for precise measurements.
338 We can distinguish another velocity change of smaller amplitude (-0.4%) in March 2010,
339 observed between 12 and 24 s of central period. This change may reflect the slip initiation of
340 the second sub-event. Unlike for the main perturbation of the velocity, the slip model

proposed by Radiguet (2011) does not have enough resolution to relate this last velocity variation to a clear episode of high slip rate. Figure 3b represents the average least-squares error on the linear regressions of *dt(t)* computed to measure the relative velocity change measure *dv/v* in the Doublet method. At the time and within periods band of the dominant perturbation, i.e. from September to November 2009 and between 12 and 24 s period, the error is stable and varies between 0.1 and 0.2% (Figure 3b). This confirms the reliability of the velocity changes observed between September and November 2009 and in March 2010.

To ensure that the measured velocity variations are independent of the variations of the noise energy, we compute the correlation coefficients between the velocity variations and the noise energy measured at 10-20 s period band. The noise energy is estimated from the squared velocities of the vertical component for stations ARIG, ATLI and APAX and then is averaged over these stations. A median filter of 40-day time window was applied to the long period noise signal. Figures 4a, b, c shows the evolution of both the noise energy and the seismic velocity variations calculated for three different period ranges 5.0-6.8 s, 13-17.9 s and 19-26 s with central period respectively of 5.9 s, 15.4 s and 22.5 s. Figure 4d summarizes the correlation coefficients for all velocity change measured for the 17 period bands listed in table 3. The correlation coefficient is close to zero at periods longer than 12 s for which we observe a velocity change. The correlation between changes in the wave speed and noise energy is somewhat higher for shorter periods between 6 and 8 s for which we do not observe velocity change during the SSE. This analysis shows that the observed seismic velocity variations are insensitive to fluctuations of the noise energy at period ranges that were used to measure them. Therefore they are likely to be related to changes of mechanical properties at depth.

### 3.2 Depth dependence of the seismic velocity changes

In order to estimate what parts of the crust are affected by the seismic velocity

perturbation, we perform an inversion of the velocity variations obtained at different period bands to obtain the velocity variation as a function of depth. Because the observed velocity changes have small amplitudes, we use a linearized approach (e.g. Aki & Richard 2002), implemented by Herrmann (2002) in his "Computer Programs in Seismology". The initial dispersion curve is computed with the 1D velocity model proposed by Campillo et al. (1996). From this velocity model we compute the phase velocity dispersion curve of Rayleigh waves. This initial dispersion curve is then modified to take into account the relative velocity changes measured previously at different period bands. After a linearized inversion of this modified dispersion curve, we obtain the S-waves relative velocity perturbation as a function of time and depth (Figure 5a). We compute the resolution matrix of the inverse problem (Figure S9) to estimate the robustness of our inversion.

The observations of wave speed variations are up to 23.50 s of central period. The resolution matrix shows that this gives a satisfactory resolution down to 20 km and thus we can see that the velocity perturbation does not affect the first 10 km of the crust (Figure 5a). Figure S10 shows the perturbation of S-wave velocity as a function of depth at four dates indicated as i, j, k, l in Figure 5a. This inversion of the velocity changes at depth shows that the shallow part of the crust is not involved in the velocity decrease that maximizes in the mid-lower crust.

### 3.3 Elastic modeling of the 2009-2010 SSE

The velocity perturbation at periods longer than 12 s reaches its maximum in October 2009 and then recovers to its average value after 2 months. On the other hand, the first sub-event of the 2009-2010 SSE slip sequence lasted approximately 8 months and the second sub-event lasted 6 months. Rapid relaxation of the velocity perturbation in comparison with the

389 slip duration suggests that the change in wave speed in not related directly to the strain
390 produced by the SSE.

391 To better understand the origin of the velocity change in term of perturbation of the
392 mechanical properties, we computed a quasi-static time evolution of the three-dimensional
393 elastic strain field associated with the 2009-2010 SSE. We used an elastic 3D finite-difference
394 code (Olsen *et al.* 2009) with the following model settings: the 2D velocity structure below
395 the Guerrero province (Iglesias *et al.* 2010), the geometry of the subduction interface
396 determined from receiver function analysis (Perez-Campos *et al.* 2008), and the slip model of
397 the 2009-2010 SSE (Radiguet 2011). We focus in particular on volumetric strain or dilation
398 because it affects both the velocities of P and S waves that form Rayleigh waves.

399 We perform a spatial average of the dilation beneath our seismic network for each depth.
400 We then average over the 40-day time window to obtain the daily rate of the dilation
401 presented in Figure 5c. We observe that the maximum rate of dilation occurred from
402 September to November 2009, at the time when the seismic velocity perturbation reached its
403 maximum (Figure 5a). In addition, the duration of the velocity perturbation is of the same
404 order of the duration of the high strain rate episode. Another variation of seismic wave speed
405 is observed at the time of the slip initiation of the second sub-event (March 2010) that is also
406 associated with an increase in the dilation rate. In this case, the dilation rate remains high and
407 lasts longer than the velocity perturbation. However, the slip model is not accurate enough to
408 resolve well a low amplitude slip at the beginning of the second sub-event slip sequence.
409 Nevertheless a relationship between seismic velocity changes and strain rate produced by the
410 SSE is rather evident. Rivet *et al.* (2011) observed the same correlation for the 2006 SSE in
411 Guerrero region using a dataset from a different seismic network (the Meso American
412 Seismic Experiment). The observed velocity variations suggest that mechanical properties of
413 the upper plate are affected by the strain rate changes produced during the SSE. Based on

these observations, we propose to use temporal velocity anomalies at depth as a proxy of the strain rate changes in the overriding plate crust.

### 3.4 Relation between the seismic velocity changes and the non-volcanic tremors

In section 3.3 we argued that the velocity changes could be seen as a proxy of strain rate in the crust. If this hypothesis is true, it may imply some relations between velocity changes and other transient phenomenon such as non-volcanic tremors (NVT). In this section, we further investigate the relation between the observed seismic velocity changes and the NVT activity at the seismic station ARIG (see map Figure 1). The NVT energy is estimated from the squared velocities of the vertical component and is dominant in the frequency band between 2 and 7 Hz (Figure 5b). Two different median filters were applied to the time series. The first one is a short 4-day median filter that highlights short duration high energy NVT activity. The second median filter, calculated on 40-day time windows, is used in order to compare NVT activity with both variations in seismic velocity perturbation and volumetric strain estimated in the same period of time. This long time window avoids the influence of short and very strong events (e.g., Kostoglodov *et al.* 2010; Husker *et al.* 2010; Zigone *et al.* 2012). From mid-September to December 2010, the level of activity is high compared to the baseline level of the background activity (about 50 decibels). This period of high activity coincides with both the drop in seismic velocity produced by the first sub-event (Figure 5a), and the maximum strain rate (Figure 5c). This suggests that the tremor activity, along with a decrease in seismic wave velocity, is related to the slip rate at the interface during the SSE. However, several periods of strong tremor activity are observed at other times for which slip is not clearly detected. These activities have characteristic durations of the order of ten days, shorter than the duration of the NVT high activity during the velocity change observed from mid-

September to December. It can be noted that moderate SSE (Mw < 6) can hardly be distinguished in GPS time series.

To evaluate carefully the relation between velocity changes and NVT activity we compare the evolution of the seismic velocity changes with the median NVT energy, both estimated on 40-day time windows of continuous seismic signals. We first measured the tremor activity between 2009 and 2011 from the average of the energy measured at three stations, ARIG, ATLI and APAX located in the northern part of Guerrero state, where NVTs are usually detected (Payero *et al.* 2008; Husker *et al.* 2012; Zigone *et al.* 2012) (See appendix for details). Figure 6a, b, c show the evolution of both the energy of the tremor and the seismic wave speed variations calculated for three different period ranges with central periods respectively of 5.9 s, 15.4 s and 22.5 s. Notice that the similarity between the seismic velocity change and the NVT energy variations degrades at short periods. This is illustrated in Figure 6d that shows the evolution of the correlation coefficients between changes in seismic velocity at different period bands (table 3) and energy of tremors. This measure helps to quantify the relationship between these two observables. For periods less than 12 s, the velocity variations are weakly correlated with the energy of tremors; the correlation coefficient is less than 0.4. Beyond 14 s of central period, the correlation between the two measures increases and reaches 0.7 at around 16 s. Then the correlation stabilizes at 0.6 at longer periods. This comparison confirms a close relation between the seismic velocity change and the NVT activity, in the period range for which we have identified variations in velocity produced by the SSE (i.e. between 14 and 24 s).

# 4 Discussions

## 4.1 Velocity changes associated with a complex slow slip event

The analysis of the velocity variations associated with the slow slip event of 2009-2010 shows that slow deformations affect the seismic velocities in the crust. Indeed, the maximum rate of mid-lower crustal dilation coincides with a distinctive reduction of the seismic wave velocity. A similar observation was previously reported for the 2006 SSE (Rivet *et al.* 2011), however in the case of the 2009-2010 SSE, the slip sequence was more complex. Theses new observations of velocity changes confirm the link between waves speed variations and rate of deformation.

Walpersdorf *et al.* (2011) and Radiguet (2011) showed that the first sub-event of the 2009-2011 SSE slip sequence occurred west of the seismological network with an amplitude 1.5 times larger than the second sub-event that initiated east of the network 10 months later (Figure S5). Due to the location of the seismic network relative to the slipping zones, we expected that the network would be more sensitive to perturbation related to the first rather than the second sub-event. Indeed, it appears that the change in wave speed measured during the first sub-event is larger than during the later that produced a slight decrease in the seismic velocity at its initiation in March 2010. At this time, the velocity perturbation is about three times lower than during the first sub-event. Similarly, the rate of dilation observed for the second sub-event is also about three times lower than the first sub-event. This similarity between speed variation and strain rate suggests that the velocity variations could be used as a first order indicator of the dilation rate within the crust.

## 4.2 Insights into the nonlinear behavior of the crust

The short durations of the velocity perturbation (~2 months) in comparison to the elastic

484 strain increase suggests that the velocity is not linearly related to the strain in the medium.
485 Besides the magnitude of the velocity perturbation is of the order of $10^{-3}$, while the strain
486 involved are of the order of $10^{-6}$. In linear elasticity, the velocity changes should be of the
487 same order as the dilation (see Supplementary Materials). We propose to interpret
488 observations of seismic velocity changes in the framework of nonlinear elasticity. The
489 dynamics of the rearrangement of cracks, pores and bonds between hard grains may explain
490 the decrease of elastic modulus observed in laboratory experiments on rock samples under
491 dynamic loading (Ostrovsky & Johnson 2001). The nonlinear effects are usually observed for
492 a deformation greater than $10^{-6}$ and typically produce a rapid decrease of the velocity
493 followed by a slower and gradual return to the baseline level (Johnson & Sutin 2005; Johnson
494 & Jia 2005; TenCate & Shankland 1996). These nonlinear effects may be strongly enhanced
495 by an increase in the pore pressure (Johnson & Jia 2005). In Guerrero, the typical volumetric
496 strain produced by SSE is of the order of $10^{-6}$, which is the threshold for nonlinear elastic
497 behavior in laboratory experiments. Besides, fluids released in the crust due to metamorphic
498 dehydration and high pore pressure (Jodicke et al. 2006; Song et al. 2009) could increase the
499 pore pressure and contribute to the nonlinear behavior of the crust. During SSEs, small stress
500 drop of 0.1-0.2 MPa (Radiguet *et al.* 2012), which are 10 to 100 times less than for regular
501 earthquakes, suggest high pore pressure and low effective normal stress at the subduction
502 interface. As proposed by SSE frictional models, an increase in dilation occurring
503 simultaneously with the slow slip event tends to reduce this high pore pressure at the
504 interface, and thus acts as a strengthening force, favoring steady slip (e.g. Segall *et al.* 2010)
505 and preventing the plate interface to become dynamically instable. Finally poroelasticity may
506 also contribute to the decrease of the observed seismic velocity and its recovery since it
507 affects large-scale fluid motions within the crust.

### 4.3 A complex relation between NVT and SSE

In most subduction zones where slow slip events have been detected, they are associated with non-volcanic tremor episodes. The tremor often occurs in the close vicinity of the SSE, like in Cascades (Gomberg *et al.* 2010), Nankai (Japan) (Hirose & Obara 2010), Alaska (Peterson & Christensen 2009). Bartlow *et al.* (2011) showed recently that during the 2009 SSE in Cascadia, the tremors concentrated in areas where the slow slip rate was maximal, following the slip front. The authors interpret these tremors as frictional heterogeneities that reach a slip velocity adequate for the emission of seismic waves. In Guerrero, a comparison between NVT epicenters and the area of slow slip at the subduction interface during the 2006 SSE shows that a relatively small cluster of tremors is triggered by the sliding front of the SSE, and are probably related to the shear stress accumulation (Husker *et al.* 2012). This particular NVT cluster represents only a small fraction of the entire tremor activity. In terms of seismic energy, these NVT are 2 to 3 times less energetic than those occurring farther north, outside of the 2006 SSE area (Payero *et al.* 2008; Kostoglodov *et al*. 2010; Husker *et al.* 2012). It is thus difficult to explain most of NVT in the Guerrero subduction zone by mechanical models that describe tremors as a result of frictional instabilities at the interface of the slipping zone during SSE (Obara & Hirose 2006; Shelly 2006; Shelly 2007; Ide *et al.* 2007; Kao *et al.* 2007; Brown *et al.* 2009; Ghosh *et al.* 2009; La Rocca *et al.* 2009; Larmat *et al.* 2009). Seismological and geodetic observations in Guerrero do not support this model and different explanations are needed to explain the spatial and energetic nonconformity of NVT associated to SSEs.

### 4.4 Relation between NVTs, SSE and seismic velocity changes

In Guerrero, the observations of a reduction of the seismic velocity extending at depth in the crust during the SSEs in 2006 and 2009-2010 indicate that the crust undergoes volumetric

strain rate high enough to induce nonlinear elastic response. The analysis of the 2009-2010 SSE shows that there is a significant correlation between the NVT activity and the variations of the seismic wave speeds suggesting that these two different and independent observations can be linked to a single mechanism. The correlation between velocity change and NVT energy suggests that the increase in dilatation caused by the SSE can produce simultaneously the drop of velocity within the crust and enhanced NVTs activity, either at the subduction interface or on secondary faults and cracks in the crust. This activity could be linked to changes of effective pressure during the SSE as suggested by recent mechanical models involving dilatancy (Segall *et al*, 2010). Furthermore high rate dilation can affect areas away from the slipping plate interface and therefore might enhance NVT activity distant from the main fault (SSE slipping zone).

For the periods without large SSEs, Vergnolle et al. (2010) and Zigone *et al*. (2012) highlighted the coincidence of high strain rate periods, as revealed by careful analysis of GPS time series, with the occurrence of NVTs. Zigone et al. (2012) showed that the increase of non-volcanic tremor activity in Guerrero was associated with some peaks of displacement velocity of the American plate in the southern direction, indicative of slow slip episodes.

The correlation between temporal variations in seismic speed and tremor activity (Figure 6), and their apparent relation with the 2009-2010 SSE suggests that the crustal velocity changes as well as high NVT episodes are related to the increases of strain rate associated with SSEs and can be considered as markers of the slow slip events barely detected with GPS. However the hypothesis that high frequency NVT themselves could produce a velocity decrease in the lower crust cannot be discarded. Recent laboratory experiments (Johnson et al., 2012) suggest that insonation at high frequency of a rock sample produces a reduction of the elastic parameters. Further quantitative studies are needed to evaluate the expected threshold of amplitude for the non-elastic behavior and to evaluate how far the shaking from

tremor could be responsible for a velocity reduction.

# 5 Conclusion

The results obtained in this study are in good agreement with those obtained previously for the 2006 Guerrero slow slip event and confirm that the crust presents a non-linear behavior when subject to relatively low strain. Through the study of waves speed variations produced by the 2009-2010 slow slip event, we show that the relative velocity change is a robust measure that is correlated with the dilation rate at depth.

With the new data acquired during the 2009-2010 SSE, we study simultaneously changes in wave velocity and the energy of non-volcanic tremors. A good correlation between NVTs activity and velocity changes during 2009-2011 suggest a relation between the deformation of the overriding plate and the NVTs. A joint analysis of these various observations highlights the importance of the strain increase within the crust, which is associated with velocity decrease and NVT occurrence. These observations suggest that both NVTs and seismic speed variation can be used as a proxy of the strain rate at depth.

# 6 Acknowledgments

This study was supported by the Agence National de la Recherche (France) under the contract RA0000CO69 “G-GAP”, by the European Research Council Advanced Grant 227507 «Whisper » and by project grants form CONACYT 84544 and PAPIIT IN110611 and IN103808. We are grateful to all people who participated in the seismic antennas installation and maintenance. We thank Paul Johnson and other G-GAP participants (Allen Husker, Guillaume Bacques) for their stimulating discussions. We thank Catherine Pequegnat and Ekaterina Bourova-Flin for their work on the management of the seismological database.

# References


Aki, K. & Richards, P., 2002. *Quantitative Seismology,* University Science Books.

Altamimi, Z., Collilieux, X., & Métivier, L., 2011. Itrf2008: an improved solution of the international terrestrial reference frame, *Journal of Geodesy,* **85**(8), 457–473.

Bartlow, N., Miyazaki, S., Bradley, A., & Segall, P., 2011. Space-time correlation of slip and tremor during the 2009 Cascadia slow slip event, *Geophysical Research Letters*, **38**(18), L18309.

Brenguier, F., Campillo, M., Hadziioannou, C., Shapiro, N. M., Nadeau, R. M., & Larose, E., 2008a. Postseismic relaxation along the San Andreas fault at Parkfield from continuous seismological ob- servations, *Science*, **321**(5895), 1478–1481.

Brenguier, F., Shapiro, N. M., Campillo, M., Ferrazzini, V., Duputel, Z., Coutant, O., & Nercessian, A., 2008b. Towards forecasting volcanic eruptions using seismic noise, *Nature Geoscience*, **1**(2),126–130.

Brown, J. R., Beroza, G. C., Ide, S., Ohta, K., Shelly, D. R., Schwartz, S. Y., Rabbel, W., Thorwart, M., & Kao, H., 2009. Deep low-frequency earthquakes in tremor localize to the plate interface in multiple subduction zones, *Geophysical Research Letters*, **36**, L19306.

Brown, K., Tryon, M., DeShon, H., Dorman, L., & S., S., 2005. Correlated transient fluid pulsing and seismic tremor in the Costa Rica subduction zone, *Earth and Planetary Science Letters*, **238**(1-2), 189–203.

Campillo, M. & Paul, A., 2003. Long-range correlations in the diffuse seismic coda, *Science*, **299**(5606), 547–549.

Campillo, M., Singh, S., Shapiro, N., Pacheco, J., & Herrmann, R., 1996. Crustal structure south of the Mexican volcanic belt, based on group velocity dispersion, *Geofisica Internacional - Mexico*, **35**, 361-370.

Chen, J. H., Froment, B., Liu, Q. Y., & Campillo, M., 2010. Distribution of seismic wave speed changes associated with the 12 May 2008 Mw 7.9 Wenchuan earthquake, *Geophysical Research Letters*, **37**, L18302

Clarke, D., L. Zaccarelli, N.M. Shapiro, and F. Brenguier, Assessment of resolution and accuracy of the Moving Window Cross Spectral technique for monitoring crustal temporal variations using ambient seismic noise, Geophys. J. Int., 186, 867–882.

612 Delahaye, E. J., Townend, J., Reyners, M. E., & Rogers, G., 2009. Microseismicity
613 but no tremor accompanying slow slip in the Hikurangi subduction zone, New
614 Zealand, *Earth and Planetary Science Letters*, **277**(1-2), 21–28.
615 DeMets, C., Gordon, R. G., Argus, D. F., & Stein, S., 1994. Effect of recent
616 revisions to the geomagnetic reversal time-scale on estimates of current plate
617 motions, *Geophysical Research Letters*, **21**(20), 2191–2194.
618 Froment, B., Campillo, M., Roux, P., Gouedard, P., Verdel, A., & Weaver, R. L.,
619 2010. Estimation of the effect of nonisotropically distributed energy on the
620 apparent arrival time in correlations, *Geophysics*, **75**(5), SA85–SA93.
621 Ghosh, A., Vidale, J. E., Sweet, J. R., Creager, K. C., & Wech, A. G., 2009. Tremor
622 patches in Cascadia revealed by seismic array analysis, *Geophysical Research*
623 *Letters*, **36**, L17316.
624 Gomberg, J. et al., 2010. Slow-slip phenomena in Cascadia from 2007 and beyond:
625 A review, *Geological Society of America Bulletin*, **122**(7-8), 963–978.
626 Hadziioannou, C., Larose, E., Coutant, O., Roux, P., & Campillo, M., 2009.
627 Stability of monitoring weak changes in multiply scattering media with ambient
628 noise correlation: Laboratory experiments, *Journal of the Acoustical Society of*
629 *America*, **125**(6), 3688–3695.
630 Hennino, R., Tregoures, N., Shapiro, N., Margerin, L., Campillo, M., van Tiggelen,
631 B., & Weaver, R., 2001. Observation of equipartition of seismic waves, *Physical*
632 *Review Letters*, **86**(15), 3447–3450.
633 Herrmann, R., 2002. Computer programs in seismology, version 3.15, *Saint Louis*
634 *University*, Saint Louis, Mo.
635 Hillers, G., Graham, N., Campillo, M., Kedar, S., Landès, M., & Shapiro, N.,
636 2012. Global oceanic microseism sources as seen by seismic arrays and predicted
637 by wave action models, *Geochemistry Geophysics Geosystems*, **13**, Q01021.
638 Hirose, H. & Obara, K., 2010. Recurrence behavior of short-term slow slip and
639 correlated Nonvolcanic tremor episodes in western Shikoku, southwest Japan,
640 *Journal of Geophysical Research*, **115**, B00A21.
641 Hirose, H., Asano, Y., Obara, K., Kimura, T., Matsuzawa, T., Tanaka, S. & Maeda, T.,
642 2010. Slow earthquakes linked along dip in the Nankai subduction zone, *Science,*
643 **330**(6010), 1502.
644 Husker, A., Peyrat, S., Shapiro, N., & Kostoglodov, V., 2010. Automatic
645 non-volcanic tremor detec- tion in the Mexican subduction zone, *Geofisica*

646 *Internacional - Mexico*, **49**(1), 17–25.
647 Husker, A., Kostoglodov, V., Cruz-Atienza, V., Legrand, D., Shapiro, N., Payero,
648 J., Campillo, M., & Huesca-Pérez, E., 2012. Temporal variations of non-volcanic
649 tremor (NVT) locations in the Mexican subduction zone: finding the NVT sweet
650 spot, *Geochemistry Geophysics Geosystems*, **13**, Q03011.
651 Ide, S., Shelly, D. R., & Beroza, G. C., 2007. Mechanism of deep low frequency
652 earthquakes: Further evidence that deep non-volcanic tremor is generated by
653 shear slip on the plate interface, *Geophysical Research Letters*, **34**, L03308.
654 Iglesias, A., Clayton, R. W., Perez-Campos, X., Singh, S. K., Pacheco, J. F.,
655 Garcia, D., & Valdes- Gonzalez, C., 2010. S wave velocity structure below
656 central Mexico using high-resolution surface wave tomography, *Journal of*
657 *Geophysical Research-Solid Earth*, **115**(B6), B06307.
658 Jodicke, H., Jording, A., Ferrari, L., Arzate, J., Mezger, K., & Rupke, L., 2006.
659 Fluid release from the subducted Cocos plate and partial melting of the crust
660 deduced from magnetotelluric studies in southern Mexico: Implications for the
661 generation of volcanism and subduction dynamics, *Journal of Geophysical*
662 *Research-Solid Earth*, **111**, B08102.
663 Johnson, P. & Sutin, A., 2005. Slow dynamics and anomalous nonlinear fast
664 dynamics in diverse solids, *Journal of the Acoustical Society of America*, **117**(1),
665 124–130.
666 Johnson, P. A. & Jia, X., 2005. Nonlinear dynamics, granular media and dynamic
667 earthquake triggering, *Nature*, **437**(7060), 871–874.
668 Johnson, P. A.,Carpenter, B., Knuth, M., Kaproth, B. M., Le Bas, P.-Y., Daub, E. G.
669 & Marone, C., 2012. Nonlinear dynamical triggering of slow slip on simulated
670 earthquake faults with implications to Earth, Journal of Geophysical Research,
671 **117**(B04), B04310, doi:10.1029/2011JB008594.
672 Kao, H., Shan, S. J., Dragert, H., Rogers, G., Cassidy, J. F., & Ramachandran, K.,
673 2005. A wide depth distribution of seismic tremors along the northern Cascadia
674 margin, *Nature*, **436**(7052), 841–844.
675 Kao, H., Shan, S. J., Rogers, G., & Dragert, H., 2007. Migration characteristics
676 of seismic tremors in the northern Cascadia margin, *Geophysical Research*
677 *Letters*, **34**, L03304.
678 Kim, M. J.,Schwartz, S. Y., & Bannister, S., 2011. Non-volcanic tremor associated
679 with the March 2010 Gisborne slow slip event at the Hikurangi subduction margin,

New Zealand, *Geophysical Research Letters*, **38**(14), L14301.

Koper, K., de Foy, B., & Benz, H., 2009. Composition and variation of noise recorded at the Yellowknife seismic array, 1991–2007, *Journal of Geophysical Research*, **114**(B10), B10310.

Kositsky, A. & Avouac, J., 2010. Inverting geodetic time series with a principal component analysis- based inversion method, *Journal of Geophysical Research*, **115**(B3), B03401.

Kostoglodov, V., Husker, A., Shapiro, N. M., Payero, J. S., Campillo, M., Cotte, N., & Clayton, R., 2010. The 2006 slow slip event and nonvolcanic tremor in the Mexican subduction zone, *Geophysical Research Letters*, **37**, L24301.

La Rocca, M., Creager, K., Galluzzo, D., Malone, S., Vidale, J., Sweet, J., & Wech, A., 2009. Cascadia tremor located near plate interface constrained by S minus P wave times, *Science*, **323**(323), 620.

Landès, M., Hubans, F., Shapiro, N., Paul, A., & Campillo, M., 2010. Origin of deep ocean microseisms by using teleseismic body waves, *Journal of Geophysical Research*, **115**, B05302.

Larmat, C. S., Guyer, R. A., & Johnson, P. A., 2009. Tremor source location using time reversal: Selecting the appropriate imaging field, *Geophysical Research Letters*, **36**.

Larson, K. M., Kostoglodov, V., Miyazaki, S., & Santiago, J. A. S., 2007. The 2006 aseismic slow slip event in Guerrero, Mexico: New results from GPS, *Geophysical Research Letters*, **34**, L13309.

Lobkis, O. & Weaver, R., 2003. Coda-wave interferometry in finite solids: Recovery of p-to-s conversion rates in an elastodynamic billiard, *Physical review letters*, **90**(25), 254302.

Margerin, L., Campillo, M., Van Tiggelen, B. A., & Hennino, R., 2009. Energy partition of seismic coda waves in layered media: theory and application to Pinyon Flats Observatory, *Geophysical Journal International*, **177**(2), 571–585.

McCaffrey, R., Wallace, L., & Beavan, J., 2008. Slow slip and frictional transition at low temperature at the Hikurangi subduction zone, *Nature Geoscience*, **1**(5), 316–320.

Nugraha, A. & Mori, J., 2006. Three-dimensional velocity structure in the Bungo channel and Shikoku area, Japan, and its relationship to low-frequency earthquakes, *Geophysical research letters*, **33**(24), L24307.

714 Obara, K., 2002. Nonvolcanic deep tremor associated with subduction in southwest
715 Japan, *Science*, **296**(5573), 1679–1681.
716 Obara, K. & Hirose, H., 2006. Non-volcanic deep low-frequency tremors
717 accompanying slow slips in the southwest Japan subduction zone,
718 *Tectonophysics*, **417**(1-2), 33–51.
719 Obara, K., Hirose, H., Yamamizu, F., & Kasahara, K., 2004. Episodic slow slip
720 events accompanied by non-volcanic tremors in southwest Japan subduction
721 zone, *Geophysical Research Letters*, **31**, L23602.
722 Obara, K., 2011. Characteristics and interactions between non-volcanic tremor and related
723 slow earthquakes in the Nankai subduction zone, southwest Japan, *Journal of*
724 *Geodynamics*, **52**, 229–248.
725 Obermann, A., Planes, T., Sens-Schonfelder, C., Larose, E., & Campillo, M., 2012.
726 Depth sensitivity of coda waves to velocity perturbations in an elastic
727 heterogeneous medium, geophysical journal international. *Geophysical Journal*
728 *International*, in press, doi: 10.1093/gji/ggt043.
729 Ohta, K. & Ide, S., 2008. A precise hypocenter determination method using
730 network correlation coefficients and its application to deep low-frequency
731 earthquakes, *Earth Planets and Space*, **60**(8), 877-882.
732 Ohta, Y., Freymueller, J., Hreinsdottir, S., & Suito, H., 2006. A large slow slip
733 event and the depth of the seismogenic zone in the south central Alaska
734 subduction zone, *Earth and Planetary Science Letters*, **247**(1-2), 108–116.
735 Olsen, K. B., Day, S. M., Dalguer, L. A., Mayhew, J., Cui, Y., Zhu, J., Cruz-
736 Atienza, V. M., Roten, D., Maechling, P., Jordan, T. H., Okaya, D., &
737 Chourasia, A., 2009. ShakeOut-D: Ground motion estimates using an ensemble
738 of large earthquakes on the southern San Andreas fault with spontaneous
739 rupture propagation, *Geophysical Research Letters*, **36**, L04303.
740 Ostrovsky, L. A. & Johnson, P., 2001. Dynamic non-linear elasticity in geomaterial,
741 *Rivista del nuovo cimento*, **24**(7), 1–46.
742 Ozawa, S., Suito, H., & Tobita, M., 2007. Occurrence of quasi-periodic slow-slip
743 off the east coast of the Boso peninsula, central Japan, *Earth Planets and Space*,
744 **59**(12), 1241.
745 Payero, J. S., Kostoglodov, V., Shapiro, N., Mikumo, T., Iglesias, A., Perez-
746 Campos, X., & Clayton, R. W., 2008. Nonvolcanic tremor observed in the
747 Mexican subduction zone, *Geophysical Research Letters*, **35**, L07305.

748 Pérez-Campos, X., Kim, Y., Husker, A., Davis, P., Clayton, R., Iglesias, A.,
749 Pacheco, J., Singh, S., Manea, V., & Gurnis, M., 2008. Horizontal subduction and
750 truncation of the Cocos plate beneath central Mexico, *Geophysical Research*
751 *Letters*, **35**(18), L18303.
752 Peterson, C. L. & Christensen, D. H., 2009. Possible relationship between
753 nonvolcanic tremor and the 1998-2001 slow slip event, south central Alaska,
754 *Journal of Geophysical Research-Solid Earth*, **114**, B06302 .
755 Poupinet, G., Ellsworth, W. L., & Frechet, J., 1984. Monitoring velocity variations
756 in the crust using earthquake doublets - An application to the Calaveras fault,
757 California, *Journal of Geophysical Research*, **89**(NB7), 5719–5731.
758 Radiguet, M., 2011. Etude des séismes lents et du chargement intersismique dans
759 la lacune sismique de Guerrero au Mexique, Ph.D. thesis, Université Joseph
760 Fourier, ISTERRE.
761 Radiguet, M., Cotton, F., Vergnolle, M., Campillo, M., Walpersdorf, A., Cotte, N.,
762 & Kostoglodov, V. 2012. Slow slip events and strain accumulation in the
763 Guerrero gap, Mexico, *Journal of Geophysical Research*, **117**(B4), B04305.
764 Rivet, D., Campillo, M., Shapiro, N. M., Cruz-Atienza, V., Radiguet, M., Cotte,
765 N., & Kostoglodov, V., 2011. Seismic evidence of nonlinear crustal deformation
766 during a large slow slip event in Mexico, *Geophysical Research Letters*, **38**,
767 L08308.
768 Rogers, G. & Dragert, H., 2003. Episodic tremor and slip on the Cascadia
769 subduction zone: The chatter of silent slip, *Science*, **300**(5627), 1942–1943.
770 Rubinstein, J., Shelly, D., & Ellsworth, W., 2010. Non-volcanic Tremor: A
771 Window into the Roots of Fault Zones, in New Frontiers in Integrated Solid
772 Earth Sciences, edited by S. Cloetingh, and J. Negendank, pp. 287–314, Springer,
773 Dordrecht, Netherlands..
774 Schimmel, M., Stutzmann, E., Ardhuin, F., & Gallart, J., 2011. Polarized earth's
775 ambient microseismic noise, *Geochemistry Geophysics Geosystems*, **12**(7),
776 Q07014.
777 Schwartz, S. & Rokosky, J., 2007. Slow slip events and seismic tremor at circum-
778 pacific subduction zones, *Reviews of Geophysics*, **45**, RG3004.
779 Segall, P., Rubin, A., Bradley, A., & Rice, J., 2010. Dilatant strengthening as a
780 mechanism for slow slip events, *Journal of Geophysical Research*, **115**, B12305.
781 Shapiro, N. & Campillo, M., 2004. Emergence of broadband Rayleigh waves from

782 correlations of the ambient seismic noise, *Geophysical Research Letters*, **31**,
783 L07614.
784 Shelly, D. R., Beroza, G. C., Ide, S., & Nakamula, S., 2006. Low-frequency
785 earthquakes in Shikoku, Japan, and their relationship to episodic tremor and
786 slip, *Nature*, **442**(7099), 188–191.
787 Shelly, D. R., Beroza, G. C., & Ide, S., 2007. Non-volcanic tremor and low-
788 frequency earthquake swarms, *Nature*, **446**(7133), 305–307.
789 Song, T. R. A., Helmberger, D. V., Brudzinski, M. R., Clayton, R. W., Davis, P.,
790 Perez-Campos, X., & Singh, S. K., 2009. Subducting Slab Ultra-Slow Velocity
791 Layer Coincident with Silent Earthquakes in Southern Mexico, *Science*,
792 **324**(5926), 502–506.
793 Stehly, L., Campillo, M., & Shapiro, N. M., 2006. A study of the seismic noise from
794 its long-range correlation properties, *Journal of Geophysical Research-Solid*
795 *Earth*, **111**, B10306.
796 Stutzmann, E., Schimmel, M., Patau, G., & Maggi, A., 2009. Global climate
797 imprint on seismic noise, *Geochemistry Geophysics Geosystems*, **10,** Q11004.
798 Tanimoto, T., Ishimaru, S., & Alvizuri, C., 2006. Seasonality of particle motion of
799 microseisms, *Geophysical Journal International*, **166**, 253–266.
800 Walpersdorf, A., Cotte, N., Kostoglodov, V., Vergnolle, M., Radiguet, M., Antonio
801 Santiago, J., & Campillo, M., 2011. Two successive slow slip events evidenced in
802 2009-2010 by a dense GPS network in Guerrero, Mexico, *Geophysical Research*
803 *Letters*, **38**, L15307.
804 Weaver, R. & Lobkis, O., 2001. Ultrasonics without a source: Thermal fluctuation
805 correlations at MHz frequencies, *Physical Review Letters*, **87**, 134301.
806 Weaver, R., Froment, B., & Campillo, M., 2009. On the correlation of non-
807 isotropically distributed ballistic scalar diffuse waves, *Journal of the Acoustical*
808 *Society of America*, **126**(4), 1817–1826.
809 Weaver, R. L., Hadziioannou, C., Larose, E., & Campillo, M., 2011. On the
810 precision of noise corre- lation interferometry, *Geophysical Journal*
811 *International*, **185**(3), 1384–1392.
812 Wegler, U. & Sens-Schonfelder, C., 2007. Fault zone monitoring with passive
813 image interferometry, *Geophysical Journal International*, **168**(3), 1029–1033.
814 Zigone, D., Rivet, D., Radiguet, M., Campillo, M., Voisin, C., Cotte, N.,
815 Walpersdorf, A., Shapiro, N., Cougoulat, G., Roux, P., Kostoglodov, V., Husker,

816 A., & Payero, J., 2012. Triggering of tremors and slow slip event in guerrero,
817 mexico, by the 2010 mw 8.8 maule, chile, earthquake, *Journal of Geophysical*
818 *Research*, **117**, B09304.

# FIGURES CAPTIONS

**Figure 1** Inset: square is a study region, the Guerrero state, Mexico. Green triangles indicate the positions of broadband seismic stations (SSN) used in our analysis. The red triangles show the positions of seismic mini array network consisting of a broadband station surrounded by at least three short period sensors. The blue circles show the GPS stations. The shaded areas indicate the rupture areas of large earthquakes that occurred during the previous century. The dashed line represents the Middle America trench. The gray arrow shows the convergence rate between the Cocos and North America plates (DeMets *et al.* 1994). The colors represent the slip amplitude for the 2009-2010 SSE. Red and blue contours delimit the slip contours during the first sub-event and the second sub-event respectively (Radiguet 2011).

**Figure 2** Comparison between the seismic velocity perturbation and the 2009-2010 SSE. (a) Time series of daily north-south displacements recorded at CPDP (red) and CAYA (green) GPS stations with respect to ITRF2008 (Altamimi et al. 2011) and cumulated slip over 10 sequential days (dashed line) at the plate interface below APAX station (Radiguet 2011). (b) Seismic velocity change measured using the Doublets method from the vertical components of the correlations measured between pairs of stations at 15-20 s period band. The red bracket indicates the largest variation observed between September and November 2009. Error bars represent the average least-squares error on the linear regressions of *dt(t)* computed to measure the relative velocity change *dv/v* in the Doublet method. (c) Number of pairs of stations used to perform the velocity change measurement as a function of time. The red and green dashed lines represent respectively, the initiation of the first and second sub-event of the SSE.

**Figure 3** (a) Relative seismic velocity change (dv/v) as a function of the central period around which the correlations were filtered. The red bracket indicates the largest variation observed

between September and November 2009. (b) Average least-squares errors on the linear regressions computed to measure the relative velocity change measure dv/v (Doublet method).

**Figure 4** Comparison between the median filtered noise energy over 40-day time window measured in the 10-20 s period band (red curves) and the waves speed variation (blue curves) calculated at different period bands: 5.0-6.8 s, 13-17.9 s and 19-26 s with central period respectively of T=5.9 s (a), T=15.4 s (b) and T=22.5 s (c). The central period of the velocity variation and the correlation coefficient between the velocity variation and the noise energy measured in the 10-20 s period band are indicated on top of each plot. (d) Correlation coefficient computed between the noise energy between 10 and 20 s and the seismic velocity variations observed at different period bands.

**Figure 5** (a) S-wave relative velocity changes as a function of depth. Velocity change at time i,j,k,l are shown figure S10. (b) Non Volcanic Tremor energy at ARIG station estimated at frequency range between 2 and 7 Hz. Median filters over 4 days (blue curve) and 40-day (red curve) were applied to the noise energy. (c) Evolution of dilation per day ($\varepsilon_{ii}$ /day) averaged over a period of 20 days computed in an elastic medium from the SSE slipping model (Radiguet 2011).

**Figure 6** Comparison between the median filtered NVT energy over 40-day time window calculated between 2 and 7 Hz (red curves) and the seismic waves speed variation (blue curves) calculated at different period bands: 5.0-6.8 s, 13-17.9 s and 19-26 s with central period respectively of T=5.9 s (a), T=15.4 s (b) and T=22.5 s (c). The central period of the velocity variation and the correlation coefficient between the velocity variation and the NVT energy are indicated on top of each plot. (d) Correlation coefficient computed between the

867 NVT energy and the seismic velocity change observed at different period bands.

868

869 **Figure 7** Comparison between the NVT energy distribution along the profile oriented
870 perpendicular to the coast and the deformation produced by the 2006 slow slip event. The
871 origin of the horizontal axis is the coast position in Acapulco. (a) Average NVT energy
872 between (1 and 2 Hz) during the 2006 SSE recorded by the seismic stations of the Meso-
873 American Seismic Experiment (MASE) (Kostoglodov *et al.* 2010). (b) Dilation $\varepsilon_{ii}$ and (c)
874 shear strain $\varepsilon_{xy}$ in % produced by the 2006 SSE and modeled from the SSE slip model
875 (Radiguet *et al.* 2011). The black line shows the subduction interface (Perez-Campos et al.
876 2008) and the thick pink line indicates the portion of the interface that slipped during the 2006
877 SSE.

878

# FIGURES

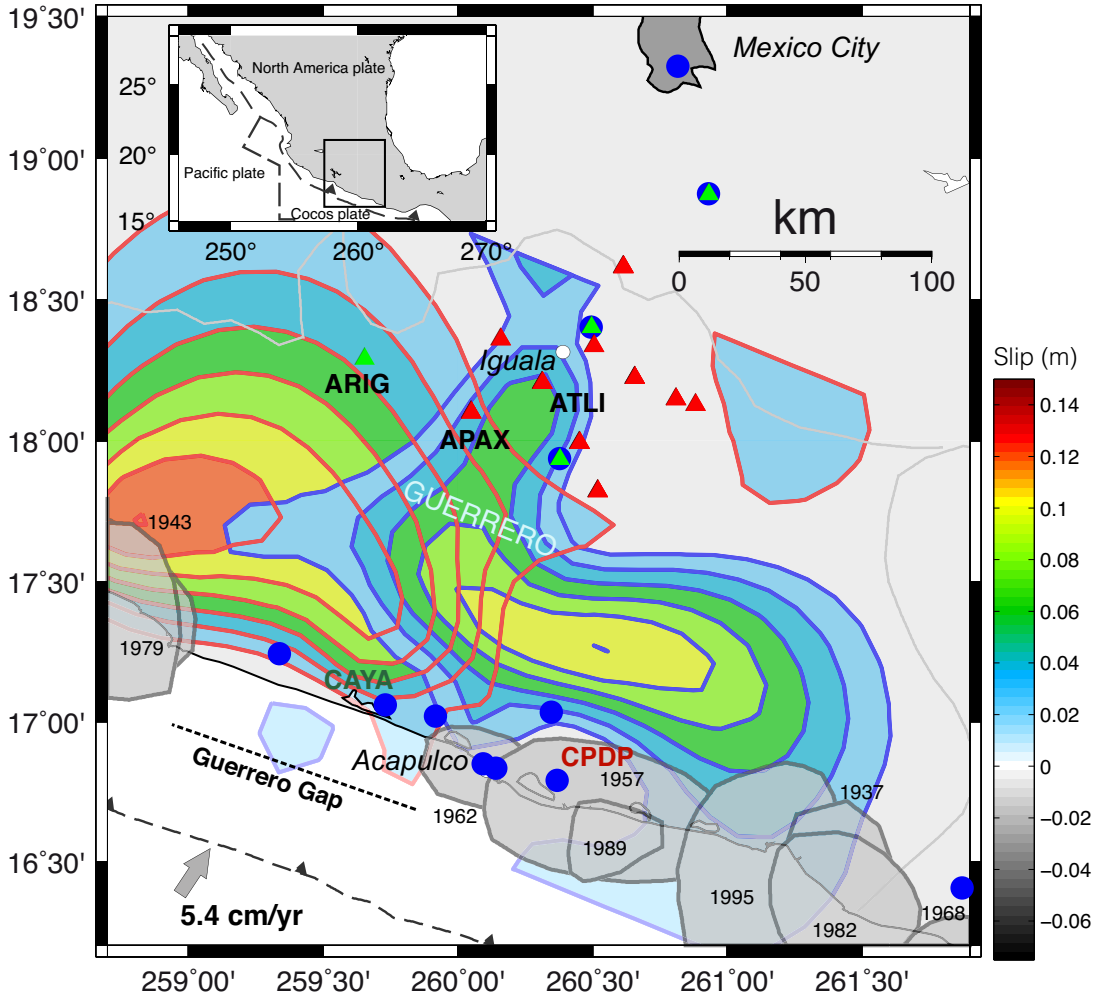


**Figure 1**

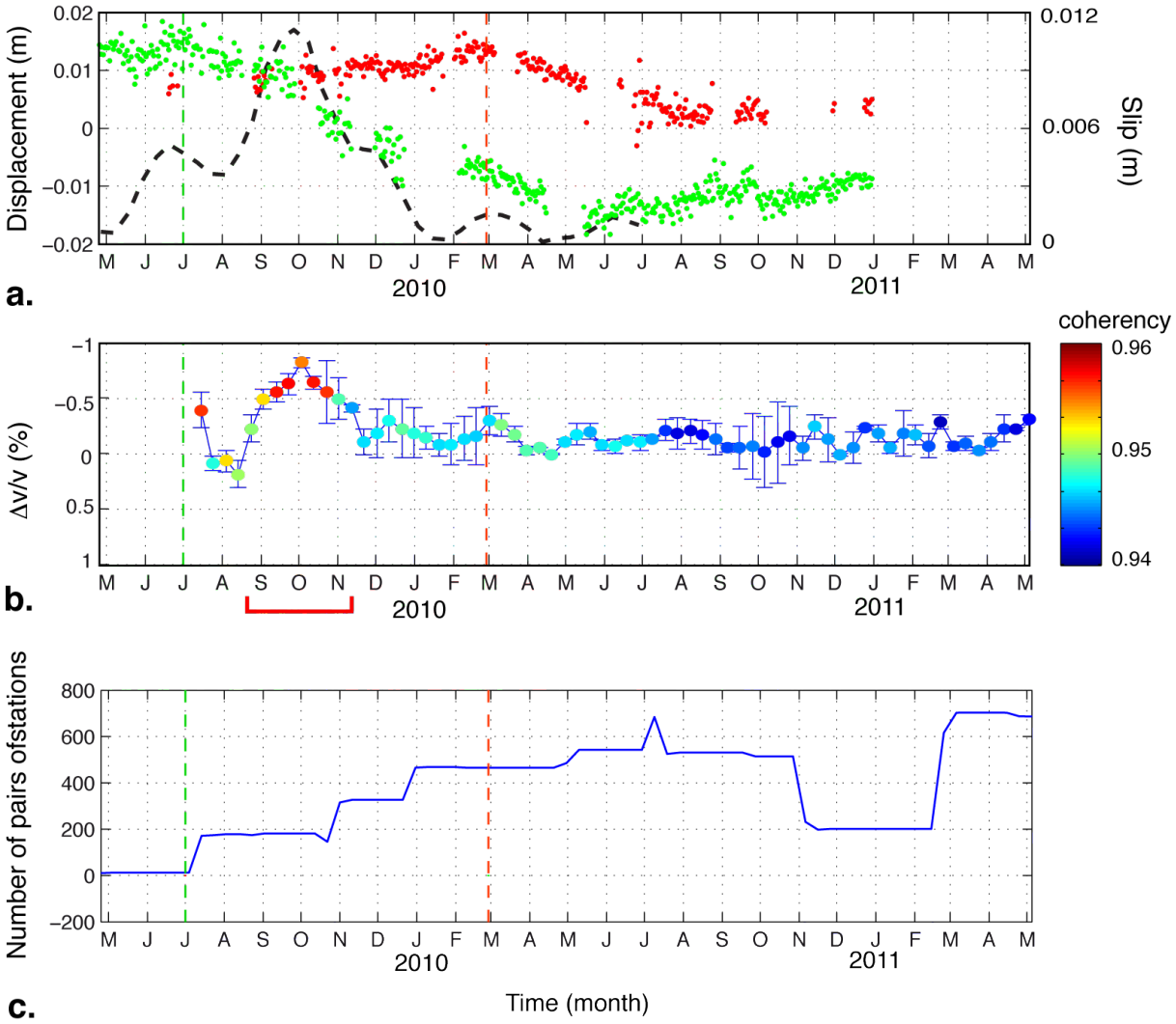
Displacement (m)
Slip (m)
a.
2010
2011
Δv/v (%)
coherency
b.
Number of pairs ofstations
c.
Time (month)

**Figure 2**

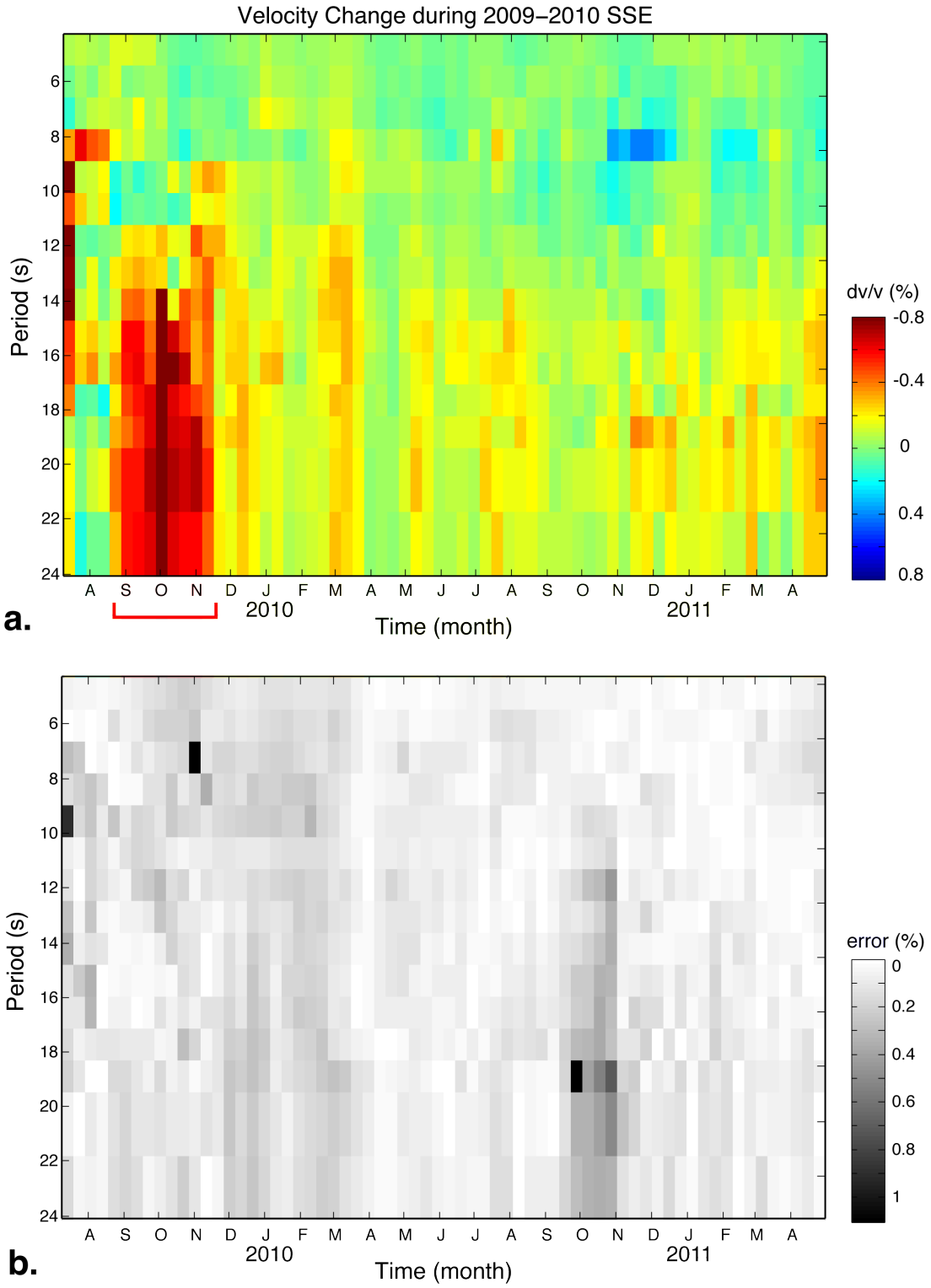


885

886 **Figure 3**

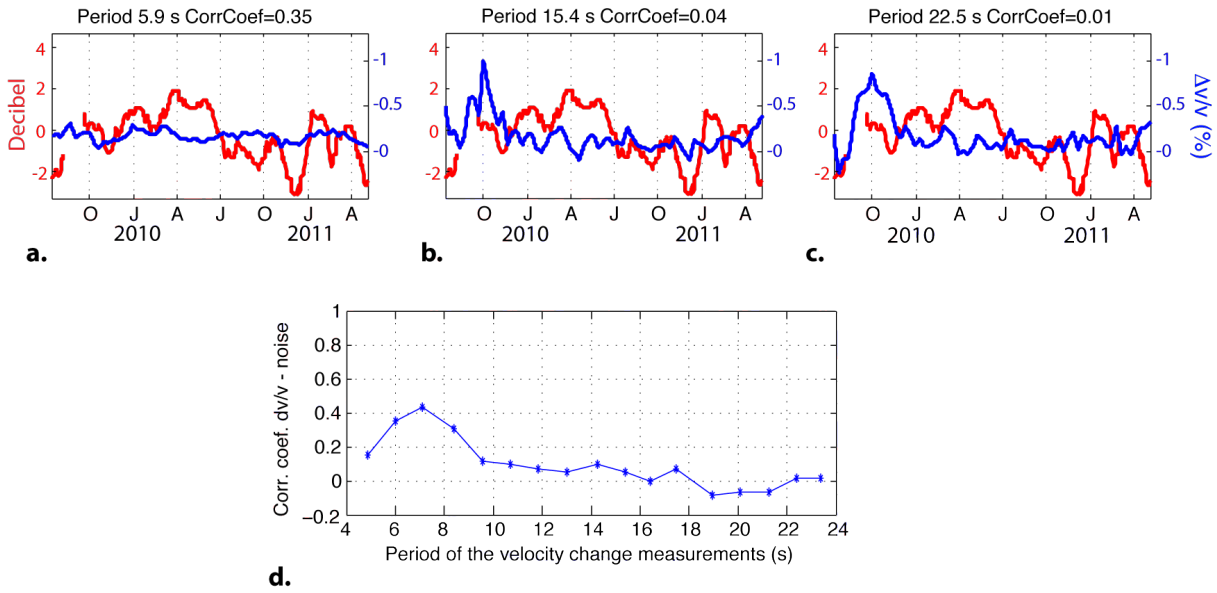


887

888 **Figure 4**

889

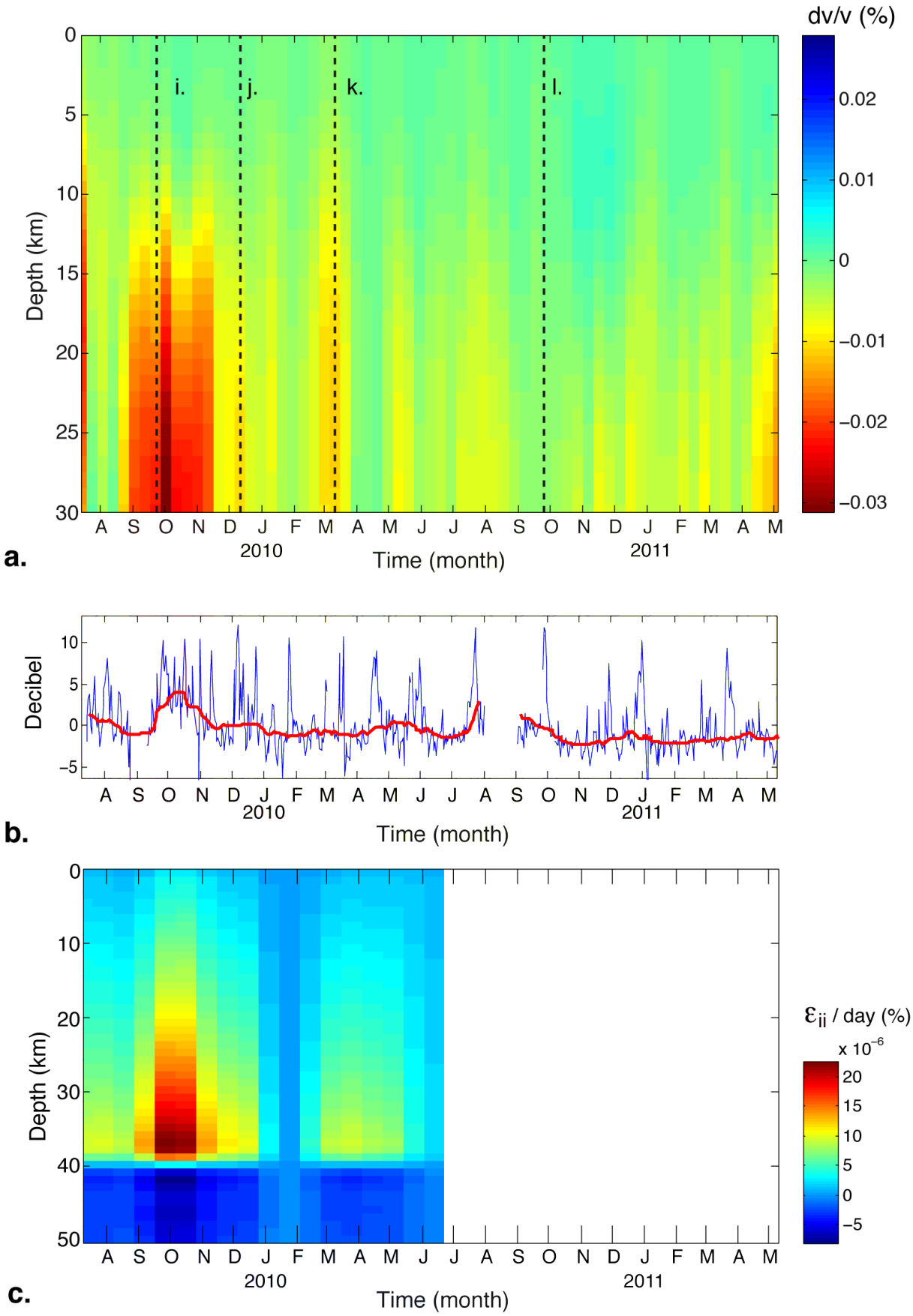
dv/v (%)
0.02
0.01
0
−0.01
−0.02
−0.03
Depth (km)
i.
j.
k.
l.
A S O N D J F M A M J J A S O N D J F M A M
2010
2011
Time (month)
a.
Decibel
Time (month)
b.
Depth (km)
$\varepsilon_{ii}$ / day (%)
x $10^{-6}$
20
15
10
5
0
−5
Time (month)
c.

**Figure 5**

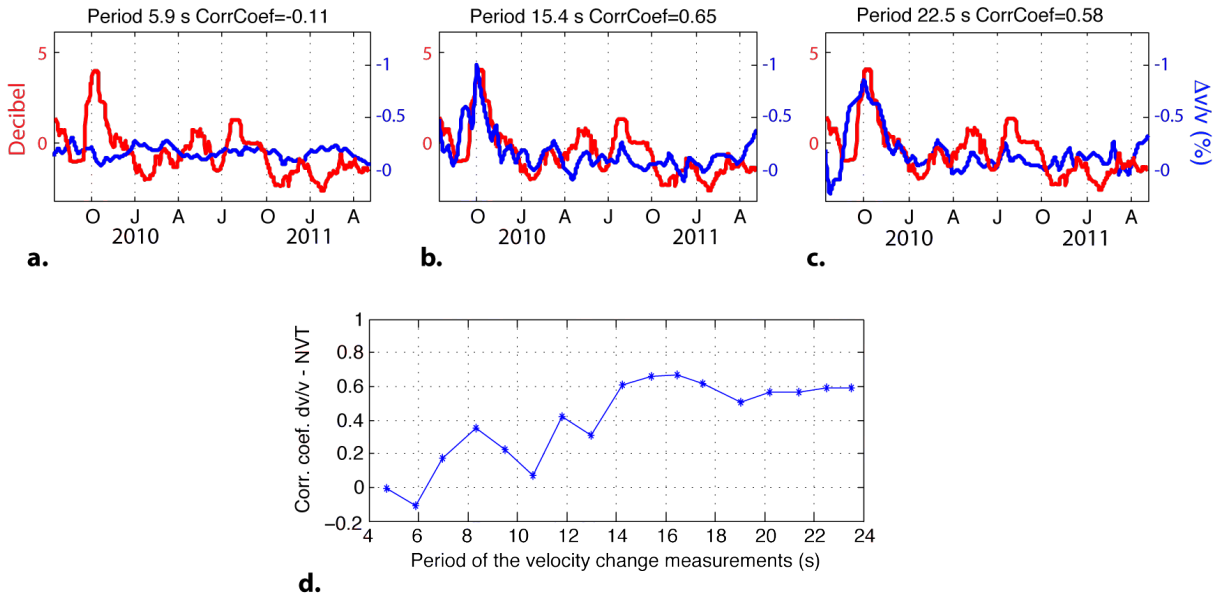


**Figure 6**

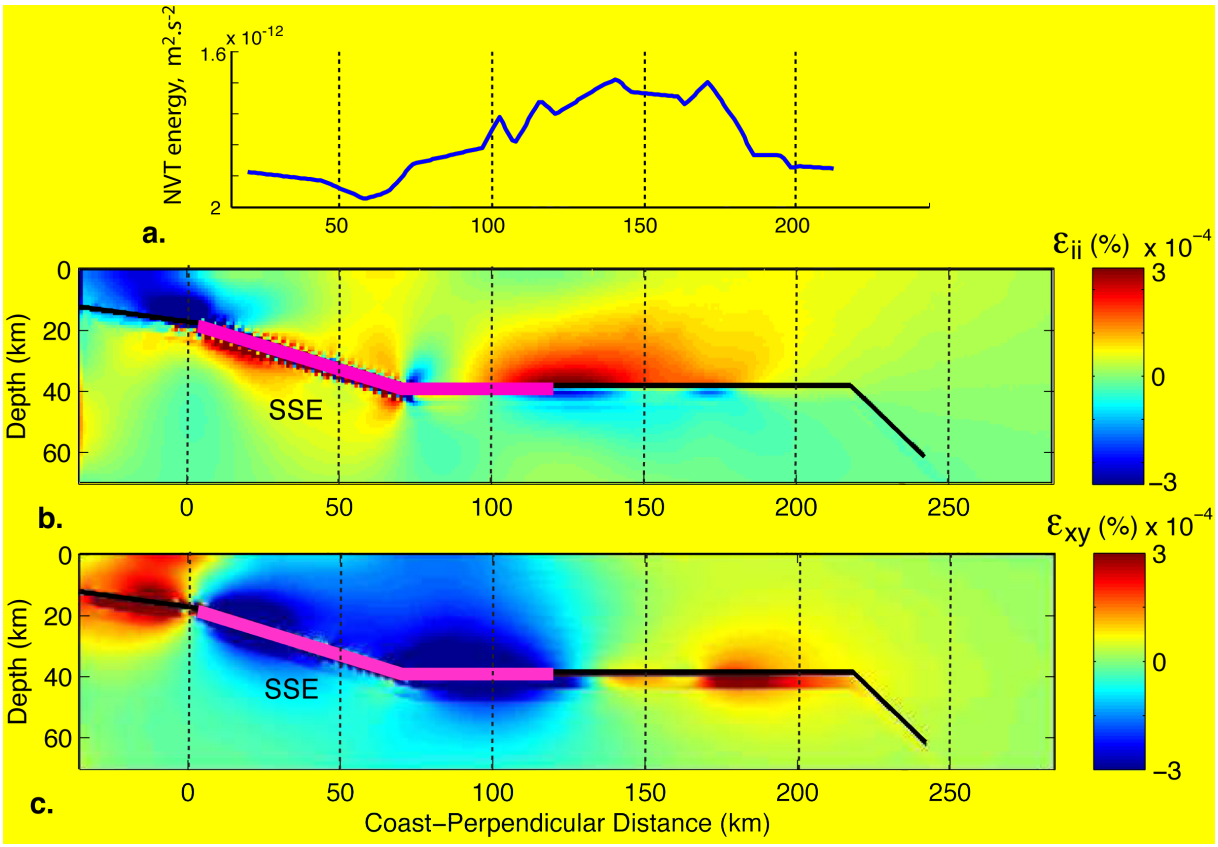


**Figure 7**

# TABLES

| Station Name G-GAP array | Latitude (°N) | Longitude (°E) | Number of Broadband sensors | Number of Short period sensors |
|---|---|---|---|---|
| AMAC | 18.6066 | -99.3843 | 1 | 6 |
| APAX | 18.0913 | -99.9490 | 1 | 6 |
| ATLI | 18.1963 | -99.6853 | 1 | 6 |
| XALI | 17.9830 | -99.5471 | 1 | 6 |
| ATEN | 18.1175 | -99.1156 | 0 | 3 |
| CACA | 18.2147 | -99.3422 | 0 | 6 |
| COAC | 18.1373 | -99.1889 | 0 | 6 |
| HUIZ | 17.8119 | -99.4797 | 0 | 6 |
| TELO | 18.3500 | -99.8393 | 0 | 3 |
| TOMA | 18.3271 | -99.4933 | 0 | 3 |

898 Table 1. List of the mini-arrays of the G-GAP seismic network.

899
900

| Station Name SSN array | Latitude (°N) | Longitude (°E) |
|---|---|---|
| ARIG | 18.2805 | -100.3437 |
| MEIG | 17.9252 | -99.6197 |
| PLIG | 18.3923 | -99.5023 |
| YAIG | 18.8623 | -99.0671 |

901 Table 2. List of the broadband stations of the Mexican Seismological National Service used in

902 this study.

903

| Minimal period (s) | Maximal period (s) | Central period (s) |
|---|---|---|
| 4.0 | 5.50 | 4.75 |
| 5.0 | 6.80 | 5.90 |
| 6.0 | 8.00 | 7.00 |
| 7.0 | 9.56 | 8.28 |
| 8.0 | 11.00 | 9.50 |
| 9.0 | 12.30 | 10.65 |
| 10.0 | 13.70 | 11.85 |
| 11.0 | 15.15 | 13.07 |
| 12.0 | 16.50 | 14.25 |
| 13.0 | 17.90 | 15.45 |
| 14.0 | 18.90 | 16.45 |
| 15.0 | 20.00 | 17.50 |
| 16.0 | 22.00 | 19.00 |
| 17.0 | 23.30 | 20.15 |
| 18 .0 | 24.70 | 21.35 |
| 19.0 | 26.00 | 22.50 |
| 20.0 | 27.00 | 23.50 |

904 Table 3. List of period bands used to filter cross-correlations before measuring velocity

905 changes.